Arch. Metall. Mater. **67** (2022), 2, 623-635

DOI: https://doi.org/10.24425/amm.2022.137799

ZHU-WEN YAN[1], BAO-SHENG WANG[1], HE-NAN BU[2*], HAO LI[1],
LEI HONG[1], DIAN-HUA ZHANG[3]

COMPREHENSIVE ANALYSIS OF METAL DEFORMATION LAW BASED ON NUMERICAL SIMULATION OF COLD ROLLING PROCESS

Through taking the cold rolling process as the research object, the three-dimensional finite element model of the strip rolling process is established by using ANSYS/LS-DYNA software. The actual rolling product data has strong consistency with the finite element simulation results. The rolling process is dynamically simulated, and the distribution curves of important rolling parameters such as equivalent stress, control efficiency coefficient, transverse rolling pressure, lateral thickness and work roll deflection is obtained. Based on summarizing the influence of rolling parameters on rolling deformation, the research results of this paper can play an important role in the actual rolling process control. The research results have certain guiding significance for the development and optimization of the rolling control system.

Keywords: 3D elastic-plastic FEM; work roll deflection; lateral thickness; flatness regulation effect; rolling pressure

Introduction

Coupling analysis of roll elastic deformation and strip deformation is a necessary method to study the deformation process of cold rolling. Low computational efficiency is inevitable in the elastic-plastic finite element calculation process using implicit static iterative algorithm. It is not easy to converge when the contact problem of large deformation is analyzed. Based on the simulation results, the peak value of rolling pressure and the location of the peak were analyzed under different rolling conditions by Xiang-hua Liu [1]. A 3D elastic-plastic finite element method (FEM) model of cold strip rolling for 6-high continuous variable crown (CVC) control rolling mill was developed by Kezhi Linghu [2]. Qing-Long Wang proposes a novel simulation approach that is applied to obtain the actuator efficiency factors in terms of work roll bending, intermediate roll bending, and intermediate roll shifting for a six-high Universal Crown Control mill (UCM mill) [3]. The distribution of rolling pressure and the change rule of lever arm coefficient under different reduction, forward and backward tension stress, deformation resistance, and friction coefficient in cold rolling are illustrated based on 3D (three-dimensional) elastic-plastic FEM (finite element model) simulation by Jie Sun [4]. Because the explicit time integration is used during the calculation process, no iterative solution is needed in the explicit dynamics and the computational efficiency is high. The elastoplastic deformation of the strip during rolling, elastic deflection of the roll, elastic flattening and residual stress after rolling can be considered in the elastoplastic finite element method. From the relationship between IMRS and strip widths, a segmented CVC intermediate roll contour is then proposed and experimented in an industrial production by Hongbo Li [5]. Hyojin Park presents a rigorous finite element (FE) approach for 3-D coupled analysis of the elasticpastic deformation of the strip and the elastic deformation of rolls in the roll-stack of a mill stand [6]. A three-dimensional elastic-plastic finite element analysis for a strip rolling process is conducted by Qing-Long Wang when the UCM mill is subjected to different IRS values [7]. A dynamic increment model for chatter in a Universal Crown Control mill (UCM mill) is proposed by Xing Lu with the considering of strip hardening, elastic deformation of the work roll, non-linear friction, transfer delay of the strip, and dynamic coupling effect of tension between adjacent stands [8]. An improved approach based on the varying curve of crown ratio, which can give the location of the flatness defect in more detail, is proposed by

[1] NANJING INSTITUTE OF TECHNOLOGY, INDUSTRIAL TECHNOLOGY RESEARCH INSTITUTE OF INTELLIGENT EQUIPMENT, JIANGSU PROVINCIAL ENGINEERING LABORATORY OF INTELLIGENT MANUFACTURING EQUIPMENT, NANJING 211167, PEOPLES R CHINA
[2] JIANGSU UNIVERSITY OF SCIENCE AND TECHNOLOGY, SCHOOL OF MECHANICAL ENGINEERING, ZHENJIANG 212003, PEOPLES R CHINA
[3] NORTHEASTERN UNIVERSITY, STATE KEY LABORATORY OF ROLLING AND AUTOMATION, 3-11 WENHUA ROAD, SHENYANG, PEOPLES R CHINA

* Corresponding author: hnbu520@just.edu.cn

Qing-Long Wang [9]. The finite element method is widely used in the numerical simulation of rolling process. It plays an important role in calculating the rolling process parameters and improving the accuracy of the rolling model. Based on the edge drop control characters established, the control model and the cooperation strategy were designed and applied to the practical production by Xiao chen Wang [10]. The finite-element method (FEM) is used to develop the governing equation of motion of the working roll of a four-high rolling mill by Sajan Kapil [11]. A vibration model with two degrees of freedom is proposed for a cold sheet rolling mill and the stiffness parameters of different mill elements are calculated by Masoud Mosayebi [12]. Chu han Wu presents a multi-field analysis of full hydrodynamic lubrication in high speed cold rolling of metal strips [13]. In this paper, the simulation of the rolling process with relatively large ratio of width to thickness has been realized. The results are used to provide parameter predictions with reference value to the actual production.

1. Three-dimensional finite element model establishment

The method of establishing elastoplastic finite element equation considering inertial force and damping force is called dynamic analysis method [14]. The plastic processing engineering load action time is relatively short. The equations of motion including inertial and damping forces should be used [15]. When the above second-order differential equations are calculated, the center difference format is used to discrete time. Through using principle of dynamic virtual work for elastoplastic problems, the dynamic finite element equation is obtained and it is shown as equation (1).

$$[M]\{\ddot{u}\}+[C]\{\dot{u}\}+[K]\{u\}=\{P\}-\{F\} \tag{1}$$

In equation (1), $\{\ddot{u}\}$ is nodal acceleration vector. $\{\dot{u}\}$ is node velocity vector. $\{u\}$ is node displacement vector. $\{M\}$ is global concentrated mass matrix. $\{C\}$ is global damping matrix. $\{K\}$ is stiffness matrix. $\{P\}$ is external force node force vector. $\{F\}$ is internal force nodal force vector.

In order to ensure that the simulation is as close as possible to the actual rolling process, the coupling analysis of the roll system deflection, the roll elastic flattening and the strip elastic-plastic deformation are carried out. The billet has elasto-plastic deformation and work hardening during rolling, therefore a bilinear isotropic hardening model is used. The roll body has elastic deformation during rolling, so the isotropic linear material model is used. The roll neck has no deformation during rolling, so the rigid body model is used.

The unit number of the upper work roll is 100532. The unit number of the lower work roll is 100673. The unit number of upper work roll neck at operation side is 1050. The unit number of lower work roll neck at operation side is 1071. The unit number of upper work roll neck at drive side is 930. The unit number of lower work roll neck at drive side is 950. The unit number of upper intermediate roll is 21537. The unit number of lower intermediate roll is 21519. The unit number of upper intermediate roll neck at operation side is 710. The unit number of lower intermediate roll neck at operation side is 715. The unit number of upper intermediate roll neck at drive side is 750. The unit number of lower intermediate roll neck at drive side is 735. The unit number of upper backup roll is 57136. The unit number of lower backup roll is 57151. The unit number of upper backup roll neck at operation side is 1871. The unit number of lower backup roll neck at operation side is 1857. The unit number of upper backup roll neck at drive side is 1893. The unit number of lower backup roll neck at drive side is 1873. The unit number of strip is 100510. The material model of the strip is isotropic bilinear hardening model. The material model of the roll body is isotropic linear elastic model. The material

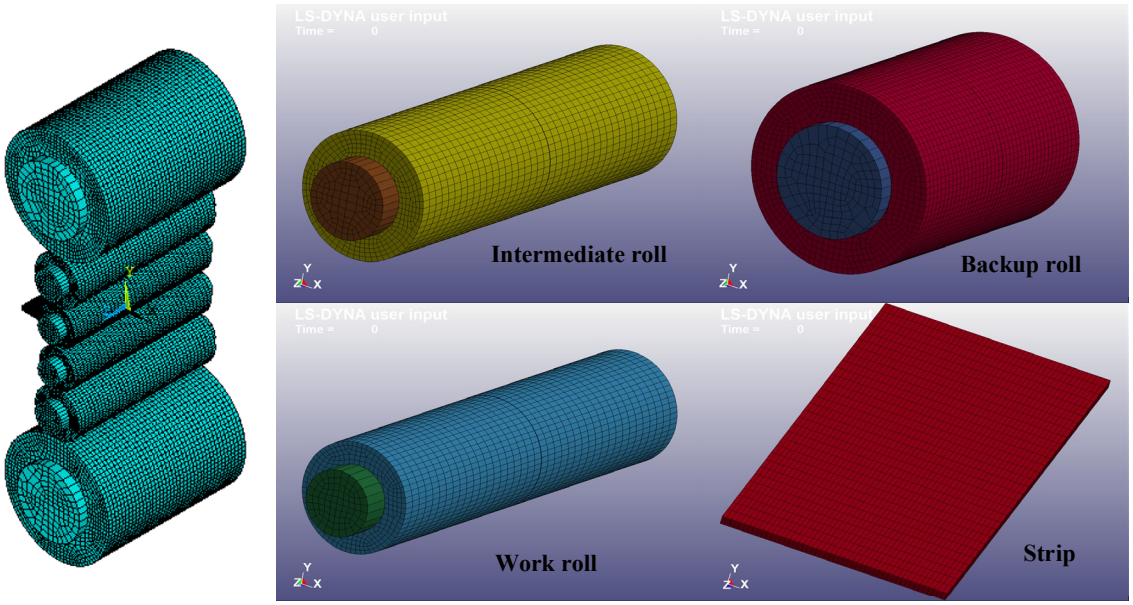

Fig. 1. Three-dimensional finite element model

model of the roll neck is rigid body model. The server type is Dell PowerEdge R740. The processor is Xeon. The number of CPU is 6. The memory is 8.00 GB.

Whether the simulation of the rolling process is accurate is of great significance to the analysis of metal flow law. The thickness distribution of the strip along the width direction is highly microscopic. In the article, the measured thickness distribution along the width of the strip is compared with the thickness distribution of the strip along the width of the finite element numerical simulation. And the two are highly consistent. Therefore, the calculation results of the finite element model established in the article are consistent with the actual situation.

Fig. 1 is a three-dimensional finite element model. The solid element of SOLOD164 three-dimensional display structure is used for finite element analysis of cold rolling process. The hexahedral mesh is adopted to mesh, and the mesh generation mode is sweep mode. In the finite element model, there are elastomer six roll system, elastoplastic strip and rigid roll neck. In this model, the bending deformation, flattening deformation and strip elastic-plastic deformation of the entire roll system are considered. Bending deformation is an important factor that directly affects the shape of the loaded roll gap. The calculation accuracy of bending deformation is critical to the simulation accuracy of the entire rolling process. It can be said that the calculation process of bending deformation directly determines the simulation results of metal flow during the rolling process.

2. Results and discussion

2.1. Rolling experiment verification of model accuracy

The original thickness of the strip used in the verification experiment is 2.8 mm. The strip width is 1250 mm. The strip type is SPCC. The rolling process parameters are shown in TABLE 1.

TABLE 1

The rolling process parameter table of verification experiment

Test group	Reduction ratio/%	Front tension/ MPa	Back tension/ MPa	Work roll bending /kN	Intermediate roll bending /kN	Intermediate roll shifting /mm
1	29.17	157.13	93.57	110.00	73.51	15
2	31.47	149.35	113.63	153.71	57.13	15

Fig. 2 is the comparison between the simulated value and the actual measured value of the lateral thickness distribution of the exit strip. The trend of measured lateral thickness distribu-

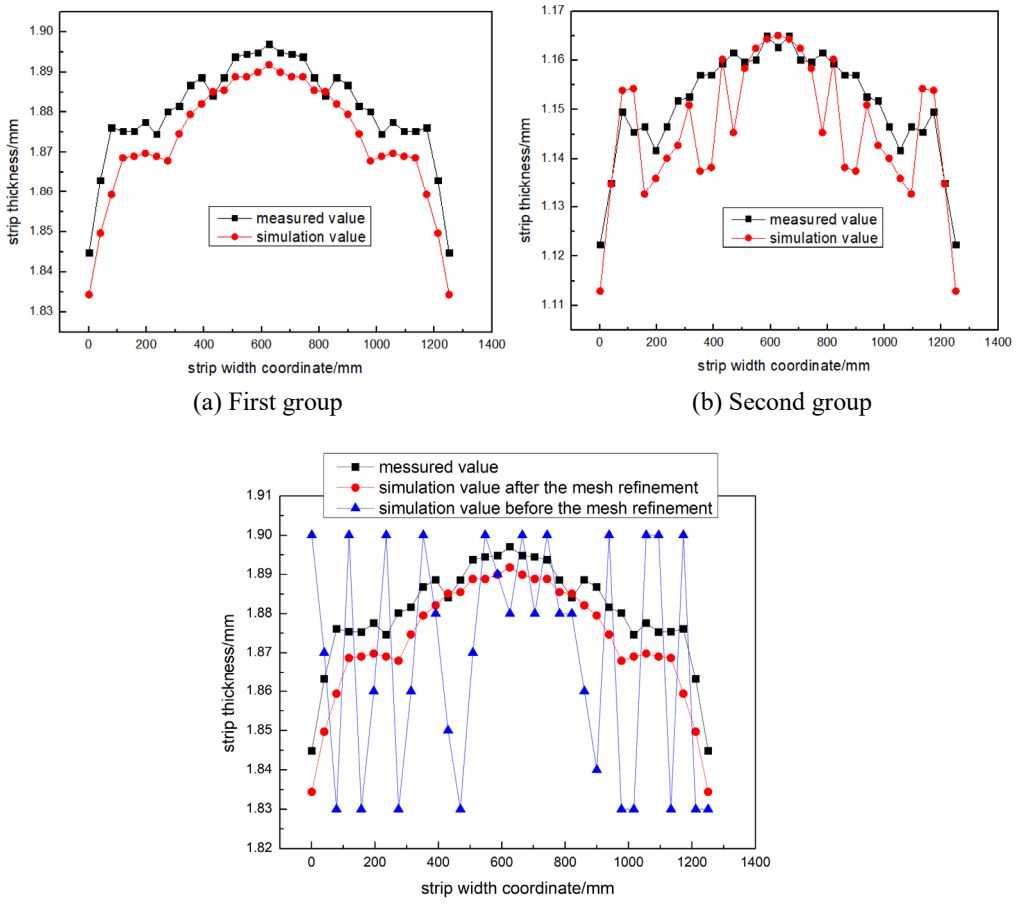

(a) First group

(b) Second group

(c) Distribution diagram of lateral thickness distribution of exit strip before and after mesh refinement

Fig. 2. Distribution diagram of finite element simulation value and actual measured value of lateral thickness distribution of exit strip

tion curve is consistent with the trend of the simulated lateral thickness distribution curve. In the verification experiment with a reduction ratio of 29.17%, the absolute error of the measured value and the simulated value does not exceed 21 um, and the relative error does not exceed 1%. In the verification experiment with a reduction ratio of 31.47%, the absolute error between the measured value and the simulated value is less than 13 um, and the relative error is less than 1%. Therefore, it is reliable to analyze the strip rolling process based on the three-dimensional finite element model of the rolling mill.

In the second group, the reduction rate is larger, and the rolling force is larger. Therefore, the error of the rolling force fluctuation along the lateral distribution is relatively large and the strip thickness fluctuation along the lateral is increased. However, the overall trend of the simulated value is consistent with the actual value. As a consequence, the simulated value has certain reference significance.

In Fig. 2(c), the simulated value of the lateral thickness after the mesh refinement has a high consistency with the actual measured lateral thickness. And the true rolling results can be reflected. At the same time, the distribution trend of the two is roughly the same. However, the distribution of the lateral thickness simulation value without mesh refinement is rather chaotic. It can be seen that the simulated value after the mesh refinement can ensure the validity of the data.

2.2. Effect of different reductions on equivalent stress

The simulation experiment parameters of the effect of different reductions on equivalent stress are shown in TABLE 2.

TABLE 2

Simulation experiment parameters of influence of reduction on equivalent stress

Test group	Strip specification /m	Reduction /m	Front tension /MPa	Back tension /MPa
1	0.038×1.2	0.00705	1.3	1.2
2	0.038×1.2	0.0105	1.3	1.2
3	0.038×1.2	0.01405	1.3	1.2

Fig. 3 is the distribution of the equivalent stress of the strip after rolling at different reductions. When the reduction is increased from 0.00705 m to 0.0105 m, the area of the large equivalent stress area is increased, and the edge of the area extends outwards more gently. At the same time, the area of the second large equivalent stress is reduced, and the edge of the area extends outward more gently. When the reduction is increased from 0.0105 m to 0.01405 m, the area of the large equivalent stress area is increased, and the edge of the area extends more violently. At the same time, the area of the second large equivalent stress is reduced, and the edge of the area extends outward more gently.

Fig. 4 is the distribution diagram of the equivalent stress of the work roll after rolling at different reductions. When the reduction is increased from 0.00705 m to 0.0105 m, the area of small equivalent stress is increased, and the edge of the area extends outwards more gently. At the same time, the area of second small equivalent stress is increased, and the edge of the area extends outwards more gently. When the reduction is increased from 0.0105 m to 0.01405 m, the area of small equivalent stress is increased, and the edge of the area extends more violently.

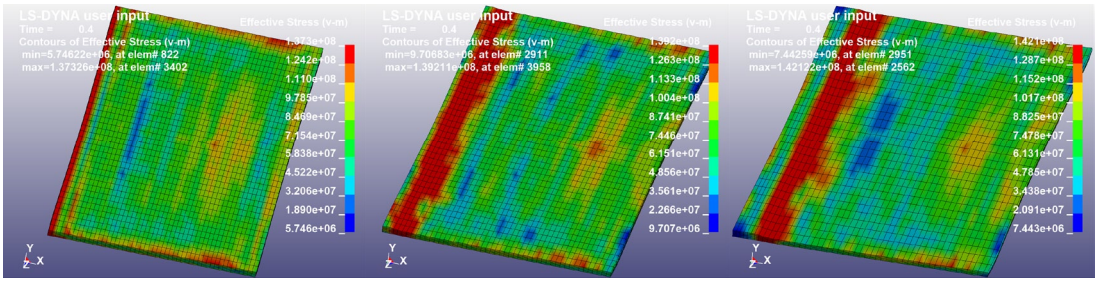

(a) Reduction 0.00705 (b) Reduction 0.0105 (c) Reduction 0.01405

Fig. 3. Distribution diagram of the equivalent stress of the strip after rolling at different reductions

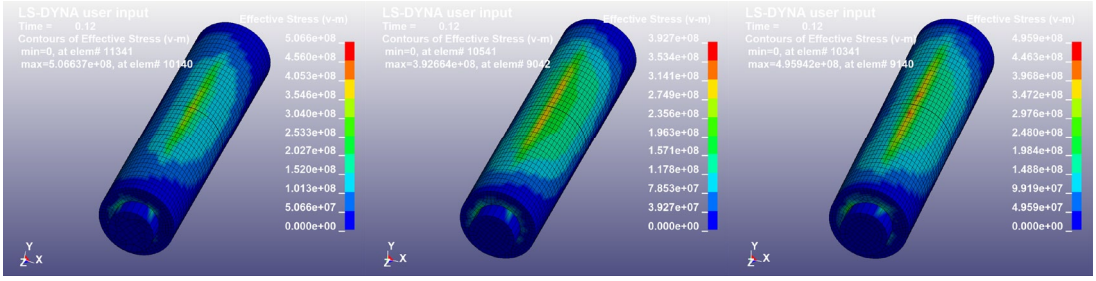

(a) Reduction 0.00705 (b) Reduction 0.0105 (c) Reduction 0.01405

Fig. 4. The distribution diagram of the equivalent stress of the work roll after rolling at different reductions

At™the same time, the area of the second small equivalent stress is reduced, and the edge of the area extends more violently.

Fig. 5 is the distribution of the equivalent stress of the intermediate roll after rolling at different reductions. When the reduction is increased from 0.00705 m to 0.0105 m, the area of small equivalent stress is reduced, and the edge of the area extends more violently. At the same time, the area of second small equivalent stress is increased, and the edge of the area extends more violently. When the reduction is increased from 0.0105 m to 0.01405 m, the area of small equivalent stress is reduced, and the edge of the area extends outwards more gently. At the same time, the area of second small equivalent stress is increased, and the edge of the area extends outwards more gently.

Fig. 6 is the distribution of the equivalent stress of the backup roll after rolling at different reductions. When the reduction is increased from 0.00705 m to 0.0105 m, the area of second small equivalent stress is reduced, and the edge of the area extends outwards more gently. When the reduction is increased from 0.0105 m to 0.01405 m, the area of second small equivalent stress is increased, and the edge of the area extends more violently.

The reduction represents the difference between the thickness of the exit and the thickness of the entry. The first group represents that the thickness of the entry minus the thickness of the exit is 0.00705 m. The second group represents that the thickness of the entry minus the thickness of the exit is 0.0105 m. The third group represents that the thickness of the entry minus the thickness of the exit is 0.01405 m.

In the analysis, the focus is on the area change of the equivalent stress distribution. The data support is provided for formulating reasonable rolling parameters by paying attention to changes of small equivalent stress and second small equivalent stress. When the reduction is increased, the effect of the increase of the large equivalent stress area on the rolling thermal crown needs to be considered. The compensation is made with roll segment cooling technology.

2.3. Analysis of the influencing factors of the regulation efficiency coefficient

The control efficiency coefficient is analyzed and calculated from the angle of the measured strip shape stress distribution [16]. The understanding of the adjustment performance of the flatness control mechanism is no longer limited to the category of the first, second, and fourth flatness deviation. Any flatness adjustment performance can be described [17]. Flatness deviation pattern recognition and decoupling calculation are not required. The flatness control effect is the amount of change in the flatness of the roll gap of the rolling mill along the strip width under the unit adjustment of a flatness control technology. It is shown in equation (2).

$$Eff_{ij} = \frac{\Delta Y_i}{\Delta U_j} \tag{2}$$

In equation (2), Eff_{ij} is flatness control efficiency coefficient. i is number of measuring points in the strip width direction. j is number of strip flatness adjustment mechanism. ΔY_i is strip flatness change amount in the i measurement section, I. ΔU_j is adjustment amount of the j strip flatness adjustment mechanism. If the adjustment mechanism is rolling force or bending force,

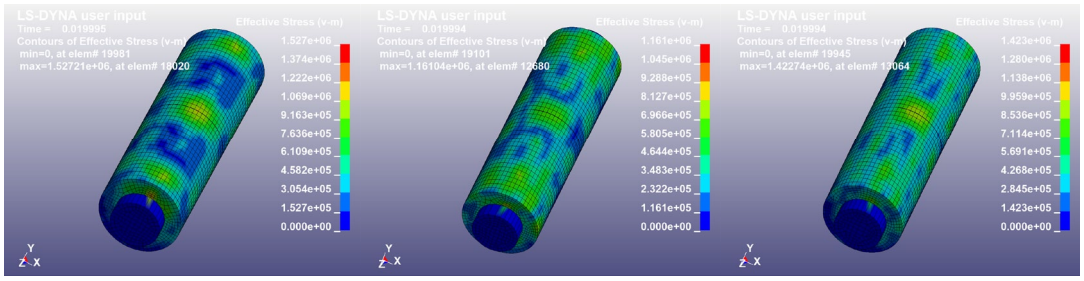

(a) Reduction 0.00705 (b) Reduction 0.0105 (c) Reduction 0.01405

Fig. 5. Distribution of the equivalent stress of the intermediate roll after rolling at different reductions

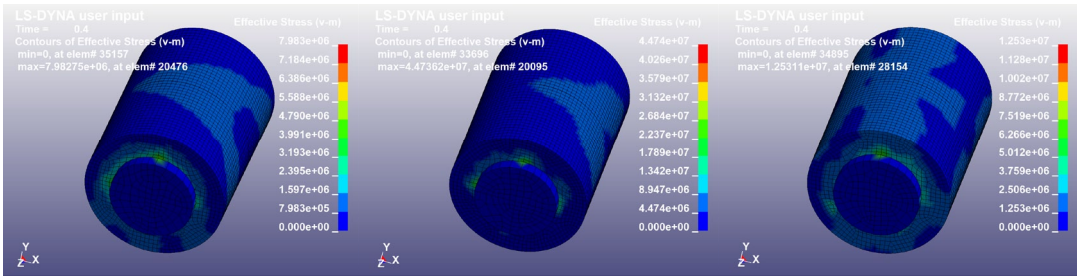

(a) Reduction 0.00705 (b) Reduction 0.0105 (c) Reduction 0.01405

Fig. 6. Distribution of the equivalent stress of the backup roll after rolling at different reductions

the unit is kN. If the adjustment mechanism is the intermediate roll shifting amount or work roll tilting amount, the unit is mm.

The roll is separated into several units. The load on the roll and the elastic deformation of the roll are discretized according to the same unit. By applying the concept of influence function in mathematical physics, the deformation caused at various points of the roll body is determined when applying unit force to each unit [18]. The deformation value of each unit is obtained by superimposing the deformation caused by each unit when all loads are applied. The influence function of work roll bending force is shown in equation (3).

$$g_{wf}(i)=\frac{1}{6E_wI_w}\left\{x_i^2(3L_w-x_i)+(1+\upsilon_w)D_w^2x_i\right\} \tag{3}$$

In equation (3), L_w is half of the work roll bending hydraulic cylinder center distance, mm. $g_{wf}(i)$ is deflection of the i unit caused by total deformation when a unit force is applied in the center of the work roll hydraulic cylinder, mm/kN. E_w is Young's modulus of work roll, kN/mm^2. I_w is modulus of bending section of work roll, mm^4. υ_w is work roll Poisson's ratio. D_w is work roll diameter, mm. x_i is i unit coordinates, mm.

2.3.1. Effect of different strip widths on bending roll efficiency coefficient

The simulation experiment parameters of the influence of different strip widths on the bending roll efficiency coefficient are shown in TABLE 3.

TABLE 3

Simulation experiment parameters of the effect of strip width on bending roll efficiency coefficient

Test group	Strip width /mm	Front tension /MPa	Back tension /MPa	Exit thickness /mm	Rolling speed /(m/min)	Reduction ratio /%
1	850	95	137	0.27	1100	15
2	950	95	137	0.27	1100	15
3	1050	95	137	0.27	1100	15
4	1150	95	137	0.27	1100	15
5	1250	95	137	0.27	1100	15

Fig. 7 is the curve distribution diagram of work roll bending efficiency coefficient at different strip widths. 20 feature points are taken in the width direction. When the strip width is increased, the regulation efficiency coefficient at the edge of the strip is increased. And when the strip width is increased, the regulation efficiency coefficient in the middle of the strip is increased. When the strip width is increased, the control effect of roll bending is enhanced. As the strip width is increased, the control ability of flatness control technology of roll bending is increased, and its regulation characteristics are particularly affected by the strip width.

2.3.2 Effect of different rolling forces on roll bending efficiency coefficient

The simulation experiment parameters of the effect of different rolling forces on the roll bending efficiency coefficient are shown in TABLE 4.

Fig. 8 is the curve distribution diagram of work roll bending efficiency coefficient at different rolling forces. 20 feature points are taken in the width direction. When the rolling force is less than 11 MN, the efficiency coefficient of the roll bending is reduced as the rolling force is increased. When the rolling force is greater than 11 MN, the efficiency coefficient of the roll bending is enhanced as the rolling force is increased. When the rolling force is above 19 MN, the coefficient of efficiency coefficient of the roll bending remains basically unchanged.

TABLE 4

The simulation experiment parameters of the effect of different rolling forces on the roll bending efficiency coefficient

Test group	Rolling force /MN	Front tension /MPa	Back tension /MPa	Exit thickness /mm	Rolling speed /(m/min)	Reduction ratio /%
1	3	75	103	0.35	1000	17
2	7	75	103	0.35	1000	17
3	11	75	103	0.35	1000	17
4	19	75	103	0.35	1000	17
5	23	75	103	0.35	1000	17

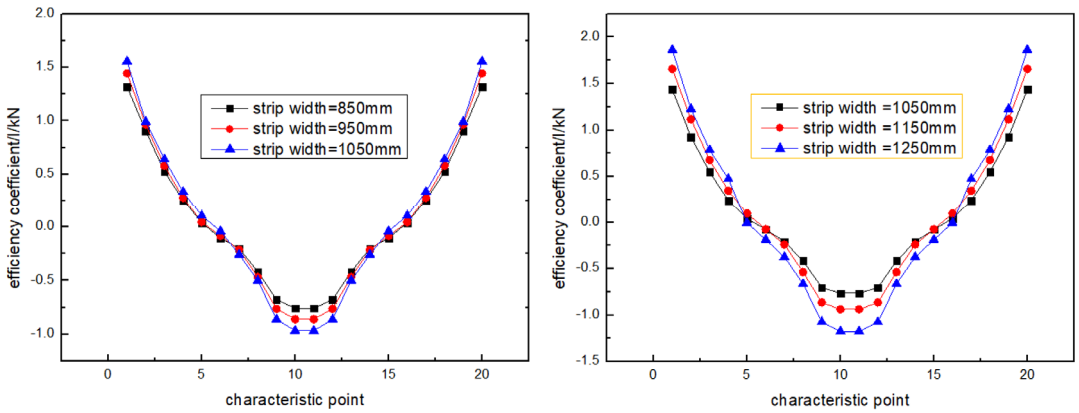

Fig. 7. Curve distribution diagram of work roll bending efficiency coefficient at different strip widths

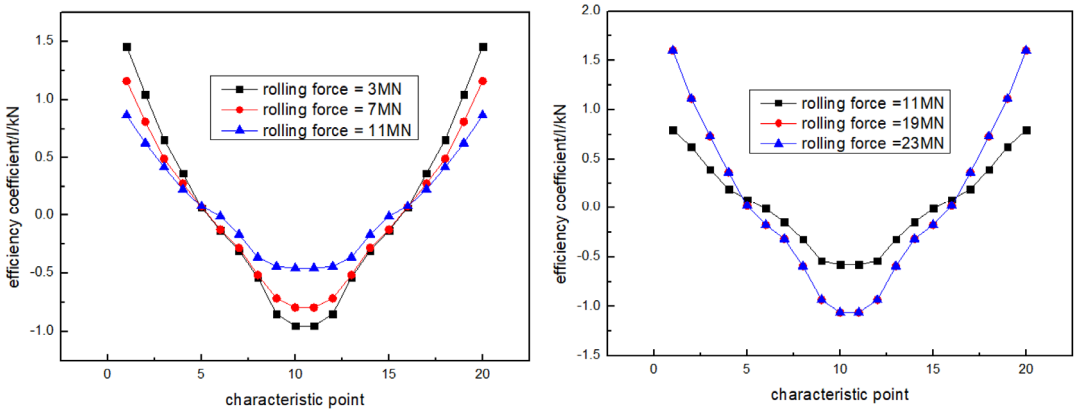

Fig. 8. Curve distribution diagram of work roll bending efficiency coefficient at different rolling forces

When it is less than a specific value, the rolling force is increased, and the effect of the work roll bending on the flatness is weakened. At this time, the gain coefficient needs to be set to compensate for the influence. When it is greater than a specific value, the rolling force is increased, and the effect of the work roll bending on the flatness is almost unchanged. Therefore, no compensation is required.

The ordinate ranges of the left and right pictures in Fig. 8 are different. This treatment is to observe the efficiency coefficients of different rolling forces more intuitively. There is a curve of rolling force = 11 MN in the left and right graphs. It serves as a reference.

2.3.3. Efficiency coefficient of different work roll bending force

The simulation experiment parameters of different work roll bending force adjustment efficiency coefficients are shown in TABLE 5.

TABLE 5

Simulation experiment parameters of the effect of work roll bending force on regulating efficiency coefficient

Test group	Work roll bending /t	Front tension /MPa	Back tension /MPa	Rolling speed /(m/min)	Reduction ratio /%
1	13	83	97	950	23
2	27	83	97	950	23
3	31	83	97	950	23
4	49	83	97	950	23

Fig. 9 is the curve distribution of the efficiency coefficient under different bending force. Δ*H* represents the change of strip thickness when the unit work roll bending force is applied. Its unit is mm/t. As the roll bending force becomes larger, the smaller, the control efficiency coefficient at the strip edge becomes smaller, and the control efficiency coefficient in the middle of the strip becomes smaller. At the same time, the™control efficiency coefficient curve becomes smoother. The 1™contro™efficienc™coefficient curve is compared with the 27t control efficiency coefficient curve. The control efficiency coefficient is decreased with the increasing of roll bending force, and it is very obvious.

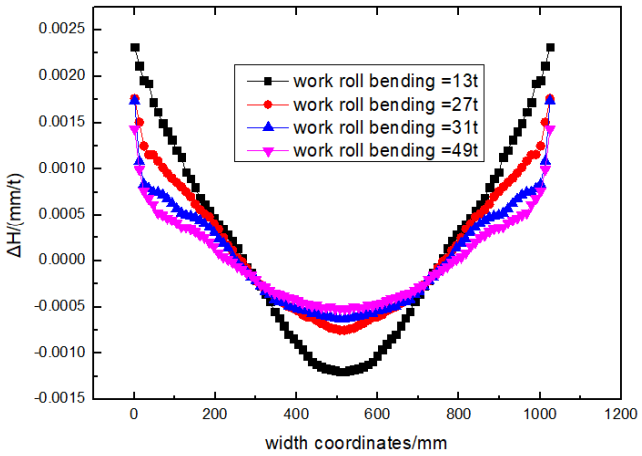

Fig. 9. curve distribution of the efficiency coefficient under different bending force

2.3.4. Efficiency coefficient of different intermediate roll bending force

The simulation experiment parameters of adjustment efficiency coefficients under different intermediate roll bending force are shown in TABLE 6.

TABLE 6

Simulation experiment parameters of adjustment efficiency coefficients under different intermediate roll bending force

Test group	Intermediate roll bending /t	Front tension /MPa	Back tension /MPa	Rolling speed /(m/min)	Reduction ratio /%
1	19	93	117	970	13
2	27	93	117	970	13
3	43	93	117	970	13
4	57	93	117	970	13

Fig. 10 is the curve distribution of the control efficiency coefficient under different rolling bending force. The control efficiency coefficient curve of the intermediate roll bending is gradually increased from the middle to the side. The control efficiency coefficient of the intermediate roll bending is also closely related to the size of the roll bending force. As the bending force is increased, the control efficiency coefficient of the intermediate roll bending roll is gradually decreased, and the distribution curve becomes more and more gentle. When the bending force is different, the efficiency coefficient at the edge of the strip is different from that at the middle of the strip. If there is no corresponding compensation function, the adjustment amount calculated by the closed loop cannot eliminate the strip flatness defects with high quality. Therefore, it is necessary to formulate the coefficient compensation function for different bending force.

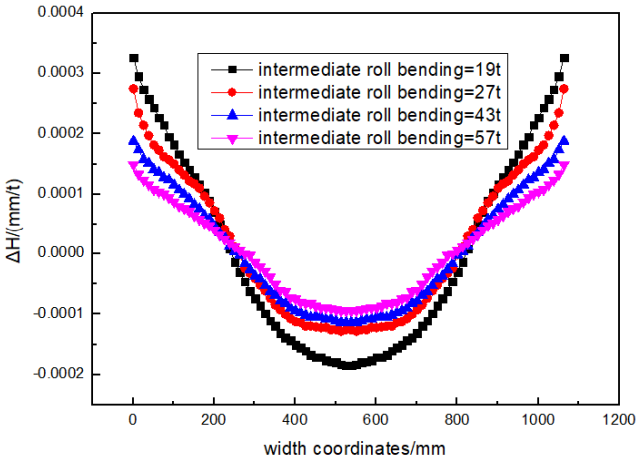

Fig. 10. curve distribution of the control efficiency coefficient under different rolling bending force

Compared with the rolling force, the influence of the bending force on the control efficiency coefficient is more complicated. Only the gain coefficient is used to compensate for this effect, and the effect is not very satisfactory. Therefore, it is necessary to use the self-learning model of the efficiency coefficient to dynamically correct the efficiency coefficient under different bending force.

2.4. Analysis of influencing factors of rolling pressure distribution along strip width

There is elastic flattening deformation in the roll and the elastic deformation in the strip. The increased part of the deformation zone is not all the plastic zone, and a considerable part is the elastic zone [19-21]. The rolling pressure in the elastic zone is much lower than the rolling pressure in the plastic zone. Due to the elastic recovery of the strip, the strip does not come out from the lowest point after the roll is flattened at the exit, but a distance higher than the lowest point [22-24]. The rolling pressure at the exit elastic zone is shown in equation (4). Fig. 11 is the diagram of elastic flattening and rolling pressure.

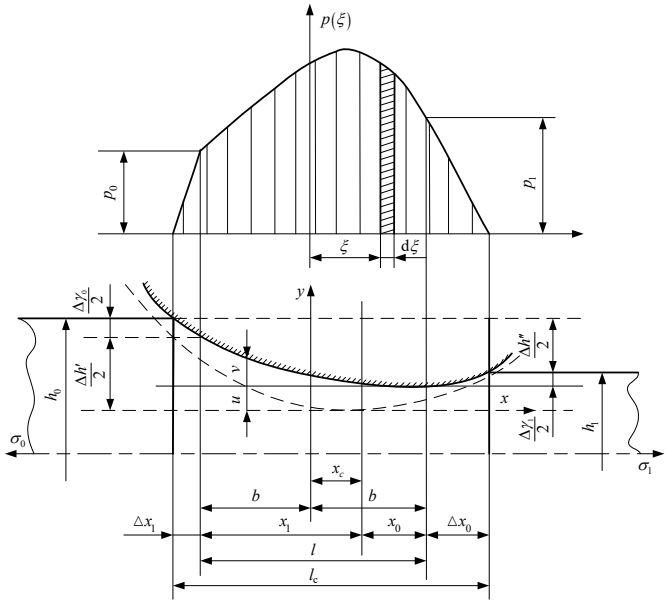

Fig. 11. Diagram of elastic flattening and rolling pressure

$$p_x = p_1 \frac{Bx-(1-B\Delta x_0)(e^{Bx}-1)}{1-(1-B\Delta x_0)e^{B\Delta x_0}} \tag{4}$$

In equation (4), p_x is rolling pressure in export elastic zone, MPa. p_1 is pressure at the beginning of the elastic zone into the plastic zone, MPa. B is constant $B=\frac{2\mu\nu}{(1-\nu)h_1}$. x is rolling direction coordinates, mm. Δx_0 is deformation zone length increment, mm.

Studying the lateral distribution of rolling pressure should consider the lateral flow of metal [25-26]. The lateral flow of metal mainly occurs in the plastic deformation zone. When the lateral distribution of rolling pressure is calculated, the longitudinal stress needs to be determined according to the longitudinal friction [27-29]. The lateral distribution of rolling pressure is shown in equation (5).

$$p(x,y)=\frac{2+\alpha}{\sqrt{1+\alpha+\alpha^2+\left(\frac{1+\alpha}{2}\right)^2\left(\frac{d\gamma_{xy}}{d\varepsilon_z}\right)^2}}K-\sigma_x \tag{5}$$

In equation (5), $p(x,y)$ is lateral distribution of rolling pressure, MPa. α is bite angle, rad. K is pure shear resistance, MPa. σ_x is x direction stress component, MPa. γ_{xy} is shear strain. ε_z is deformation in z direction.

2.4.1. Effect of work roll bending on rolling pressure distribution along strip width

The simulation experiment parameters of the influence of work roll bending on the distribution of rolling pressure along the strip width are shown in TABLE 7.

Fig. 12 is the distribution of rolling pressure along the strip width under different work roll bending forces.

TABLE 7

Simulation experiment parameters of the influence of work roll bending on the distribution of rolling pressure along the strip width

Test group	Work roll bending /kN	Front tension /MPa	Back tension /MPa	Rolling speed /(m/min)	Reduction ratio /%
1	0	73	109	870	33
2	357	73	109	870	33
3	439	73	109	870	33

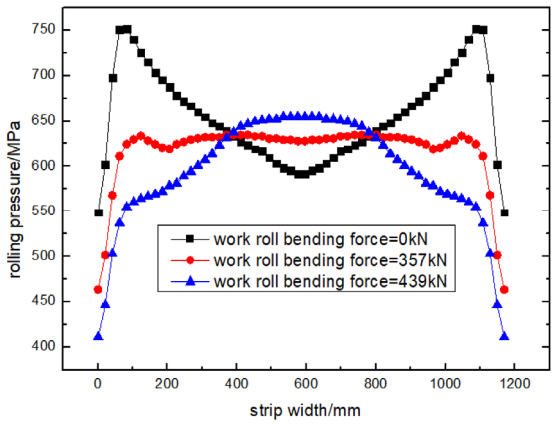

Fig. 12. Distribution of rolling pressure along the strip width under different work roll bending forces

When the work roll bending is not put in, the rolling pressure along the strip width is suddenly increased from the middle to the edge, and the peak appears. As the bending force is increased, the sudden increase trend of the rolling pressure along the strip width from the middle to the edge becomes a decrease trend, and the peak disappears.

2.4.2. Effect of intermediate roll shifting on rolling pressure distribution along strip width

The simulation experiment parameters of the influence of the intermediate roll shifting on the rolling pressure distribution along the strip width are shown in TABLE 8.

TABLE 8

Simulation experiment parameters of the influence of the intermediate roll shifting on the rolling pressure distribution along the strip width

Test group	Intermediate roll shifting /mm	Front tension /MPa	Back tension /MPa	Rolling speed /(m/min)	Reduction ratio /%
1	0	103	139	990	24
2	117	103	139	990	24
3	193	103	139	990	24

Fig. 13 is the distribution of rolling pressure along the strip width under different intermediate roll shifting. With the increase in the amount of intermediate roll shifting, the sudden increase of the rolling pressure along the strip width at the edge is gradually slowing down. The rolling pressure is also reduced along the contact arc, but the distribution trend is basically unchanged.

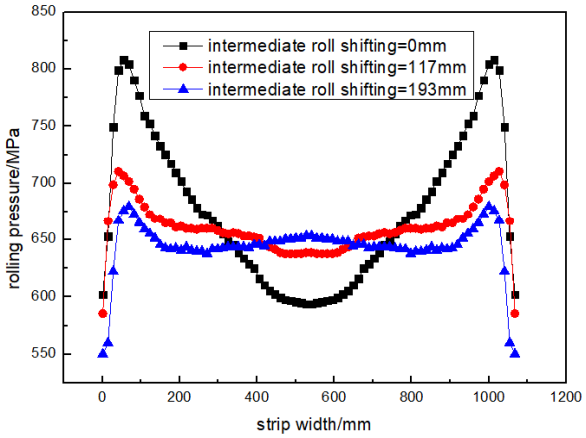

Fig. 13. Distribution of rolling pressure along the strip width under different intermediate roll shifting

2.4.3. Effect of intermediate roll bending on the distribution of rolling pressure along the strip width

The simulation experiment parameters of the influence of the intermediate roll bending on the distribution of rolling pressure along the strip width are shown in Table 9.

Fig. 14 is the distribution of rolling pressure along the strip width under different intermediate roll bending. Compared

TABLE 9

Simulation experiment parameters of the influence of the intermediate roll bending on the distribution of rolling pressure along the strip width

Test group	Intermediate roll bending /kN	Front tension /MPa	Back tension /MPa	Rolling speed /(m/min)	Reduction ratio /%
1	0	73	159	790	34
2	317	73	159	790	34
3	579	73	159	790	34

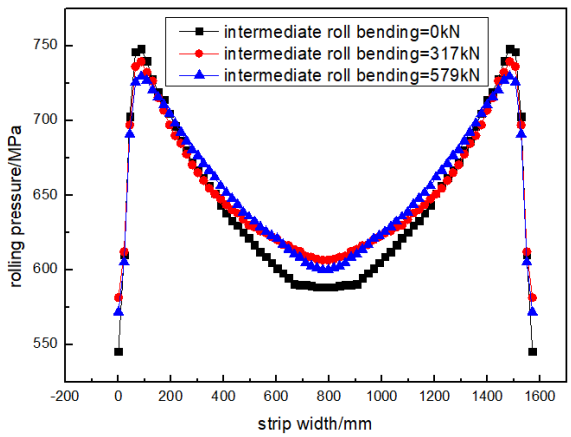

Fig. 14. Distribution of rolling pressure along the strip width under different intermediate roll bending

with the effect of work roll bending on the rolling pressure, the intermediate roll bending has little effect on it. The trend of rolling pressure distribution along the strip width has basically not changed. And the peak value is only slightly decreased, but it does not disappear.

2.5. Analysis of influencing factors of lateral thickness distribution

2.5.1. Effect of Work Roll Bending on the lateral thickness distribution of Strip Steel

The simulation experiment parameters of the influence of the work roll bending on the lateral thickness distribution of the strip are shown in TABLE 10.

TABLE 10

Simulation experiment parameters of the influence of the work roll bending on the lateral thickness distribution of the strip

Test group	Work roll bending /t	Front tension /MPa	Back tension /MPa	Rolling speed /(m/min)	Reduction ratio /%
1	0	83	127	1090	14
2	27	83	127	1090	14
3	51	83	127	1090	14

Fig. 15 is the lateral thickness distribution of strip steel for different work roll bending. As the work roll bending force becomes larger, the thickness of the central zone is increased. At the same time, with the increase of the bending force, the thickness of the edge zone is significantly increased except for the thinned area. When the bending force is 51t, the thickness of the edge is greater than the thickness of the center, and the negative convexity appears. Compared with the case without roll bending force, the shape of the strip section has a big change.

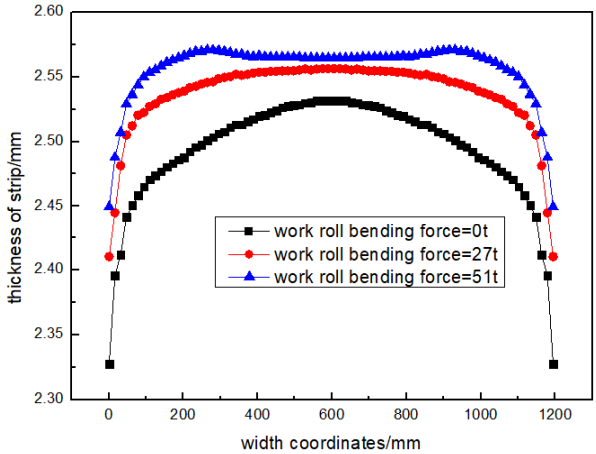

Fig. 15. Lateral thickness distribution of strip steel for different work roll bending

2.5.2. Effect of intermediate roll bending on the lateral thickness distribution of strip

The simulation experiment parameters of the influence of the intermediate roll bending on the lateral thickness distribution of the strip are shown in TABLE 11.

TABLE 11

Simulation experiment parameters of the influence of the intermediate roll bending on the lateral thickness distribution of the strip

Test group	Intermediate roll bending /t	Front tension /MPa	Back tension /MPa	Rolling speed /(m/min)	Reduction ratio /%
1	0	79	97	760	16
2	31	79	97	760	16
3	59	79	97	760	16

Fig. 16 is the lateral thickness distribution of strip steel under different intermediate roll bending. The effect of the intermediate roll bending on the shape of the strip section is small. The effect of intermediate roll bending on the thickness distribution curve is not particularly obvious. And its basic shape remains unchanged. As the bending force is increased, the thickness of the strip center is increased.

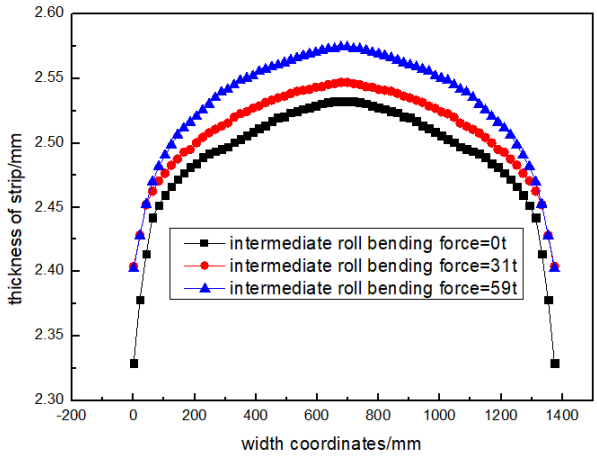

Fig. 16. Lateral thickness distribution of strip steel under different intermediate roll bending

2.6. Analysis of influencing factors of work roll deflection

The deflection of the work roll has a great influence on the strip flatness control. During the rolling process, on the one hand, the deflection of the work roll is the uneven contact deformation between the work roll and the intermediate roll and between the work roll and the strip [30]. On the other hand, because the contact length between the roll is greater than the width of the strip, the harmful contact portion makes the work roll subjected to cantilever bending. The deflection caused by the total bending deformation of the work roll is shown in equation (6).

The deflection caused by the total shear deformation of the work roll is shown in equation (7).

$$g_w^B(i,j) = \left.\frac{\partial U_b}{\partial \overline{p}}\right|_{\overline{p}=0} = \\ = \frac{l_w^3}{6E_w I_w}\left\{\left(\frac{x_j}{l_w}\right)^2\left(\frac{3x_i}{l_w} - \frac{x_j}{l_w}\right)\right\} \quad (6)$$

In equation (6), $g_w^B(i,j)$ is the deflection of the i unit caused by the total bending deformation when unit force is applied in unit j, mm/kN. U_b is total bending deformation energy, kN×mm. $\overline{p}$ is the virtual force acting on the i unit, kN. l_w is half of work roll length, mm. E_w is Young's modulus of work roll, kN/mm^2. I_w is modulus of bending section of work roll, mm^4. x_i is i unit coordinates, mm. x_j is j unit coordinates, mm.

$$g_w^s(i,j) = \left.\frac{\partial U_s}{\partial \overline{p}}\right|_{\overline{p}=0} = \frac{(1+\upsilon_w)D_w^2}{6E_w I_w}x_j \quad (7)$$

In equation (7), $g_w^s(i,j)$ is the deflection of the i unit caused by the total shear deformation when unit force is applied in unit j, mm/kN. υ_w work roll Poisson's ratio. D_w is work roll diameter, mm. U_s is total shear deformation energy, kN×mm.

2.6.1. Effect of work roll diameter on work roll deflection

The simulation experiment parameters of the influence of work roll diameter on work roll deflection are shown in TABLE 12.

TABLE 12

Simulation experiment parameters of the influence of work roll diameter on work roll deflection

Test group	Work roll diameter /mm	Front tension /MPa	Back tension /MPa	Rolling speed /(m/min)	Reduction ratio /%
1	530	113	147	960	13
2	550	113	147	960	13
3	610	113	147	960	13

Fig. 17 is the work roll deflection distribution of different work roll diameters. As the work roll diameter is decreased, the work roll deflection becomes larger within the width of the strip. The deflection distribution of the work roll in the middle is denser at different diameters. The deflection distribution of the work roll at the edge is more dispersed at different diameters. The effect of the work roll diameter on the deflection distribution of the work roll in the middle is weaker than the effect of the work roll diameter on the deflection distribution of the work roll at the edge.

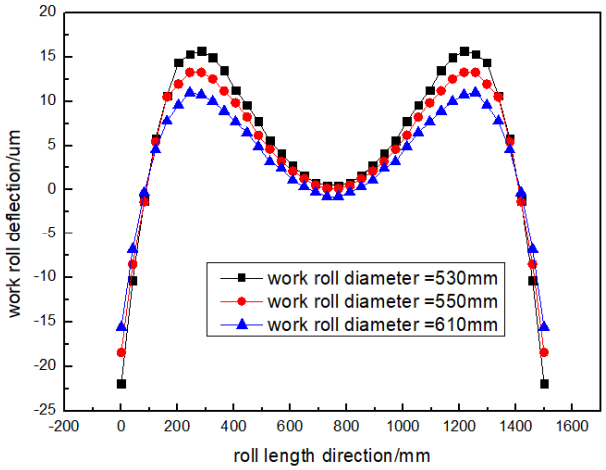

Fig. 17. Work roll deflection distribution of different work roll diameters

2.6.2. Effect of strip width on work roll deflection

The simulation experiment parameters of the influence of the strip width on the work roll deflection are shown in TABLE 13.

TABLE 13

The simulation experiment parameters of the influence of the strip width on the work roll deflection

Test group	Strip width /mm	Front tension /MPa	Back tension /MPa	Rolling speed /(m/min)	Reduction ratio /%
1	910	116	159	1200	37
2	1130	116	159	1200	37
3	1350	116	159	1200	37
4	1570	116	159	1200	37

Fig. 18 is the deflection distribution of work roll with different strip widths.

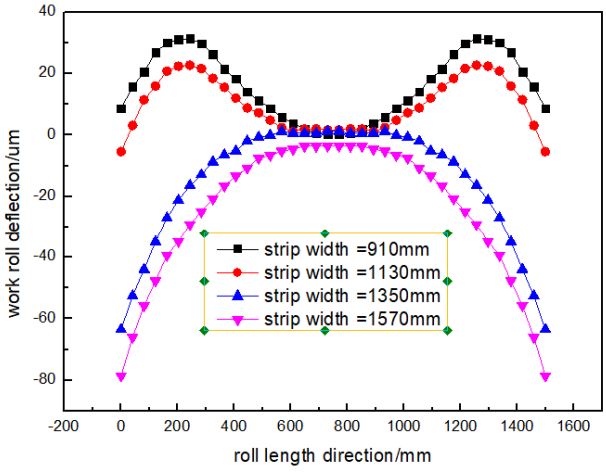

Fig. 18. The deflection distribution of work roll with different strip widths

As the strip width is increased, the deflection value of the work roll within the width of the strip becomes smaller. When the strip width is 910 mm and 1130 mm, the work roll deflection has a peak at the side, and as the strip width is increased, the peak value is decreased. When the strip width is 1350 mm and 1570 mm, the work roll deflection peak disappears at the edge and the curve becomes smooth. When the strip width is small, the work roll deflection has a peak at the edge. When the strip width is increased to a certain level, the deflection distribution curve of the work roll is gradually smoothed.

2.6.3. Effect of rolling force on work roll deflection

The simulation experiment parameters of the influence of rolling force on work roll deflection are shown in TABLE 14.

TABLE 14

Simulation experiment parameters of the influence of rolling force |on work roll deflection

Test group	Rolling force kN/mm	Front tension /MPa	Back tension /MPa	Rolling speed /(m/min)	Reduction ratio /%
1	9	106	139	1100	27
2	11	106	139	1100	27
3	15	106	139	1100	27

Fig. 19 is the deflection distribution of work roll with different rolling force. When the rolling force is increased, the deflection of the roll system is increased within the width of the strip. As the rolling force is increased, the effect of work roll deflection on the strip edge drop is increased. As the unit rolling force is decreased from 15 kN/mm to 9 kN/mm, the work roll deflection value is gradually decreased to zero.

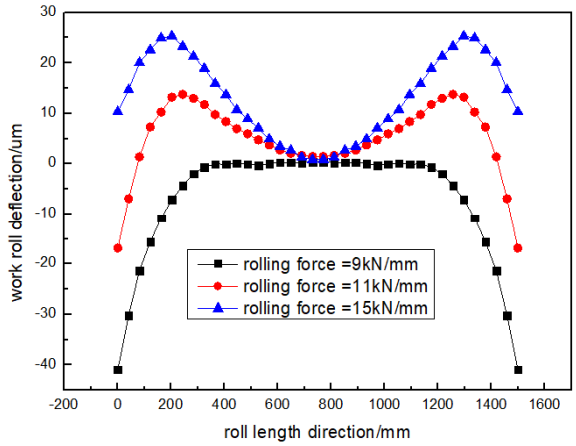

Fig. 19. Deflection distribution of work roll with different rolling force

3. Conclusion

Through finite element analysis software ANSYS/LS-DYNA, a three-dimensional simulation model of the rolling process is established. The accuracy of the model is verified by comparing and analyzing the measured and simulated values of the lateral thickness distribution. The results show that the analysis of the strip rolling process based on the three-dimensional finite element model of the rolling mill has high reliability.

The dynamic simulation of the rolling process is carried on. The main analysis content is as follows.

(1) The stress distribution of cold rolling strip at different reductions is obtained. With the increase of the reduction, the area of the large equivalent stress of the strip is increased, and the area of the second large equivalent stress of the strip is decreased.

(2) The distributions curve of control efficiency coefficients at different strip widths, rolling forces, work roll bending forces and intermediate roll bending forces is obtained. As the width of the strip is increased, the control capability of the roll bending flatness control technology is increased. After the rolling force exceeds a certain value, the control efficiency coefficient of the roll bending is basically unchanged.

(3) The rolling pressures along the width direction of different work roll bending, intermediate roll shifting and intermediate roll bending are obtained. As the bending force of the work roll is increased, the sudden increase trend of the rolling pressure in the edge zone from the middle to both sides becomes a decrease trend. As the amount of intermediate roll shifting is increased, the sudden increase trend of rolling pressure in the edge zone is slowing. With the increase of the intermediate roll bending, the rolling pressure distribution trend has not changed.

There are multivariable, strong coupling and nonlinear metal flow phenomena in the rolling process. The change law of several key rolling parameters is summarized in this article. It aims to provide effective data support for the reasonable setting of rolling process parameters. And some thoughts are provided for revealing the nature of its metal deformation.

The lateral thickness distribution of different work roll bending and intermediate roll bending is obtained. As the work roll bending force is increased, the thickness of the center strip is increased. As the bending force of the intermediate roll is increased, the thickness distribution curve changes are not particularly obvious.

The work roll deflection distribution for different work roll diameters, strip widths and rolling forces is obtained. As the work roll diameter is decreased, the work roll deflection becomes larger within the width of the strip. As the strip width is increased, the work roll deflection becomes smaller within the strip width. As the rolling force is increased, the work roll deflection becomes larger within the width of the strip.

Acknowledgments

This study is financially supported by National Key R&D Program of China (2017YFB0304100), National Natural Science Foundation of China

(No.: 51804133, 61703200), the Natural Science Foundation of Jiangsu Provincial of China (No.: BK20180977, BK20181024), and the Foundation of Nanjing Institute of Technology (No.: YKJ201867, YKJ2019112).

REFERENCES

[1] X.H. Liu, X. Shi, S.Q. Li, J.Y. Xu, G.D. Wang, Journal of Iron and Steel Research International **14**, 22-26 (2007).

[2] L. Hu, K. Zhi, Z. Y. Jiang, J. W. Zhao, F. Li, D.B. Wei, J.Z. Xu, X.M. Zhang, X.M. Zhao, The International Journal of Advanced Manufacturing Technology **74**, 1733-1745 (2014).

[3] Q.L. Wang, J. Sun, Y.M. Liu, P.F. Wang, D.H. Zhang, The International Journal of Advanced Manufacturing Technology **92**, 1371-1389 (2017).

[4] J. Sun, Y.M. Liu, Q.L. Wang, Y.K. Hu, D.H. Zhang, The International Journal of Advanced Manufacturing Technology **97**, 1847-1859 (2018).

[5] H.B. Li, Z.W. Zhao, J. Zhang, N. Kong, F. He, The International Journal of Advanced Manufacturing Technology **100**, 2387-2399 (2019).

[6] H. Park, S. Hwang, Steel Research International **88** (12), (2017).

[7] Q.L. Wang, X. Li, Y.J. Hu, J. Sun, D.H. Zhang, Steel research international **89** (5), (2018).

[8] X. Lu, J. Sun, G.T. Li, Q.L. Wang, D.H. Zhang, Journal of Materials Processing Technology **272**, 47-57 (2019).

[9] Q.L. Wang, J. Sun, X. Li, Y.M. Liu, P.F. Wang, D.H. Zhang, Journal of Manufacturing Processes **34**, 637-649 (2018).

[10] X.C. Wang, Q. Yang, H.N. He, Y.Z. Sun, Y. Liu, The International Journal of Advanced Manufacturing Technology **107**, 2497-2511 (2020).

[11] S. Kapil, P. Eberhard, K.D. Santosha, Journal of Manufacturing Science and Engineering **138** (4), (2016).

[12] M. Mosayebi, F. Zarrinkolah, K. Farmanesh, The International Journal of Advanced Manufacturing Technology **91**, 4359-4369 (2017).

[13] C.H. Wu, L.C Zhang, P.L. Qu, International Journal of Mechanical Sciences **142-143**, 468-479 (2018).

[14] H.N. Bu, Z.W. Yan, D.H. Zhang, S.Z. Chen, Scientia Iranica **23**, 2663-2672 (2016).

[15] E.J.M. Geddes, I. Postlethwaite, IEEE Transactions on Control Systems Technology **6** (2), 257-269 (1998).

[16] J.A. Polyblank, J.M. Allwood, S.R. Duncan, Journal of Materials Processing Technology, **214** (11), 2333-2348 (2014).

[17] M. Jelali, Journal of Process Control, 17 (10), 805-816 (2007).

[18] P.F. Wang, D.M. Qiao, D.H. Zhang, J. Sun, H.M. Liu, Ironmaking & Steelmaking **43** (6), 426-433 (2016).

[19] F. Zhang, A. Malik, Journal of Manufacturing Science and Engineering **140** (1), 011008-1–011008-15 (2018).

[20] Z.H. Wang, D.Y. Gong, X. Li, G.T. Li, D.H. Zhang, The International Journal of Advanced Manufacturing Technology **93**, 3325-3338 (2017).

[21] M. Rout, S.K. Pal, S.B. Singh, Journal of Manufacturing Processes **24**, 283-292 (2016).

[22] J.G. Cao, X.T. Chai, Y.L. Li, N. Kong, S.H. Jia, W. Zeng, Journal of Materials Processing Technology **252**, 432-439 (2018).

[23] Y. Zhang, Q. Yang, X.C. Wang, X.Z. Du, X. Zheng, L.S. Wang, Key Engineering Materials **443**, 21-26 (2010).

[24] B. Moazeni, M. Salimi, The International Journal of Advanced Manufacturing Technology **77**, 1315-1331 (2015).

[25] K. Yasuda, K. Narita, K. Kobayashi, I. Maeno, ISIJ International **31**, 594-598 (1991).

[26] Q.L. Wang, J. Sun, Y.M. Liu, P.F. Wang, D.H. Zhang, The International Journal of Advanced Manufacturing Technology **92**, 1371-1389 (2017).

[27] S.H. Lee, G.H. Song, S.J. Lee, B.M. Kim, Journal of Mechanical Science and Technology **25**, 2101-2109 (2011).

[28] S.J. Yoon, T.J. Shin, J.S. Lee, S.M. Hwang, Journal of Manufacturing Science and Engineering **139**, 091003-1–091003-10 (2017).

[29] P.F. Wang, D.H. Zhang, X. Li, W.X. Zhang, Steel Research International **82**, 379-387 (2011).

[30] P.F. Wang, H.F. Wang, X. Li, D.H. Zhang, W.T. Li, Y.L. Yao, Applied Mathematical Modelling **91**, 863-874 (2021).